

The impact of free convection on late morning ozone decreases on an Alpine foreland mountain summit

J.-C. Mayer¹, K. Staudt², S. Gilge³, F. X. Meixner^{1,4}, and T. Foken²

¹Biogeochemistry Department, Max Planck Institute for Chemistry, Mainz, Germany

²Department of Micrometeorology, University of Bayreuth, Bayreuth, Germany

³German Meteorological Service, Observatory Hohenpeißenberg, Hohenpeißenberg, Germany

⁴Department of Physics, University of Zimbabwe, Harare, Zimbabwe

Received: 8 January 2008 – Accepted: 13 February 2008 – Published: 17 March 2008

Correspondence to: J.-C. Mayer (jcmayer@mpch-mainz.mpg.de)

Published by Copernicus Publications on behalf of the European Geosciences Union.

5437

Abstract

Exceptional patterns in the diurnal course of ozone mixing ratio at a mountain top site (998 m a.s.l.) were observed during a field experiment (September 2005). They manifested themselves as strong and sudden decreases of ozone mixing ratio levels with a subsequent return to previous levels. Considering corresponding long-term time series (2000–2005) it was found, that such events occur mainly during summer, and affect the mountain top site in about 18% of the summer days. Combining (a) surface layer measurements at mountain summit and at the foot of the mountain, (b) in-situ (tethered balloon) and remote sensing (SODAR-RASS) measurements within the atmospheric boundary layer, the origin of these events of sudden ozone decrease could be attributed to free convection, triggered by a rather frequently occurring wind speed minimum around the location of the mountain.

1 Introduction

A sudden drop of mean mixing ratio of any trace gas species down to around 20% of its initial value is, without doubt, noticeable. If this happens at a place and time of the day, where it is not expected from present knowledge, it is worth to be studied more thoroughly. Furthermore, if such events occur frequently, it must be of considerable concern for all measurements, being made at comparable sites, as such a high frequency of occurrence could, if not filtered, affect derived statistical descriptions of the mean temporal behaviour of the trace gas.

The mean diurnal cycle (i.e. the expected course) of ozone (O_3) mixing ratio in the surface layer and at higher altitudes of the atmospheric boundary layer (ABL) is primarily dependent of the photostationary state. Within the surface layer, O_3 is depleted during night time due to deposition processes and reaction with nitrogen oxide (NO). During daytime, this process is overcompensated by NO_2 photolysis followed by O_3 production and transport of O_3 (Aneja et al., 2000). Towards higher altitudes within

5438

the ABL, these changes are less and less pronounced and are finally unimportant when reaching altitudes above possible nocturnal inversions, where O₃ mixing ratio is expected to maintain its level from the preceding day over the night (residual layer) (Aneja et al., 2000; Fast et al., 2000). However, the actual course of O₃ mixing ratio is subject to a variety of influences, from which some may be still unknown. They manifest themselves in sudden changes of mixing ratio on different time scales, ranging from minutes to days.

In general, changing O₃ levels are frequently observed and reported. Some reports deal with the expected diurnal cycle of O₃, either from ground based data (Wanner et al., 1993; Lin et al., 2004; Rummel, 2005) or from profile data (Güsten et al., 1998; Cheng, 2000). On the other hand, several studies report deviations from the “typical” behaviour. Possible reasons were found to be (a) large scale processes like frontal passages (Müller and Sladkovic, 1990), (b) changes of air masses (Strong et al., 2002), (c) mesoscale circulations like sea breezes (Hastie et al., 1999), and (d) mountain-valley circulations (Prévôt et al., 2000). Nocturnal low-level jets (LLJ) frequently cause secondary O₃ maxima during night time (Corsmeier et al., 1997; Reitebuch et al., 2000; Lee et al., 2003; Salmond and McKendry, 2002), while advection of polluted air masses has been observed as a pronounced layering in O₃ profiles in the ABL (McKendry et al., 1997; Güsten et al., 1998; Beyrich et al., 1996; McKendry et al., 1998). There are only a few reports on exceptional patterns in diurnal O₃ courses at mountain tops, and the observed deviations were always towards higher than the expected O₃ mixing ratios (Attmannspacher and Hartmannsgruber, 1973; Yelansky and Senik, 1995). For short time decreases of O₃ (0.5 to 2 h) at a mountain top, however, an explanation was not given in any of the mentioned reports. Therefore, a comprehensive set of noticeable observations at a mountain top, at the foot of the mountain and from profiles within the ABL will be used in this study to explain the origin of such short time events.

5439

2 Material and methods

2.1 The SALSA site

Our measurements have been performed during the SALSA2005 campaign (22 August 2005–23 September 2005) which took place at and around the Hohenpeissenberg (German spelling: Hohenpeißenberg), an isolated mountain (47°48' N, 11°02' E, 998 m a.s.l.) in Bavaria, southern Germany. SALSA is a German acronym, which stands for “Contribution of nitrous acid to atmospheric OH concentration”. The mountain Hohenpeissenberg is located approximately 70 km southwest of the city of Munich and 40 km north of the northern ridge of the Alps. It is covered by coniferous and mixed forest with some clearings and agriculturally used areas (managed pastures). The mountain summit overtops the surrounding area by approx. 300 m (Fig. 1). In the east of the mountain, the terrain slopes abruptly to a considerably lower level (approx. 600 m a.s.l.), while in the south the Ammer river cuts into the terrain, forming a deep canyon.

2.2 The SALSA set-up

The set-up of the field experiment has been designed to account for (a) the complex terrain, (b) the expected main regime of wind flow and (c) the existing infrastructure, i.e. the Hohenpeissenberg observatory of the German Meteorological Service (DWD), situated on top of the mountain, later referred to as the “TOP” station. All parameters measured at TOP station, being relevant for this paper, are listed in Table 1.

In addition to the TOP station, two field stations were set up. At the south-western foot of the mountain, on a managed pasture site (approx. 1.1 km from TOP, see Fig. 1), eddy covariance systems for the measurement of sensible and latent heat fluxes have been set up (BASE#1; see Table 1). Measurements of the vertical gradient of meteorological quantities and the above mentioned species have additionally been performed. The second field station was installed to monitor the state of the ABL with respect to

5440

wind velocity, turbulence intensity and thermal stratification. This site (BASE#2, see Table 1) was located directly south of the mountain (approx. 1.6 km from TOP, and approx. 1 km southeast of BASE#1), on a plateau between the mountain and the Ammer river (see Fig. 1). Two sounding systems were deployed there: (1) a SODAR-RASS system (DSDPA90.64, METEK, with 1.29 GHz RASS extension), providing vertical profiles (20 m resolution) of wind velocity, fluctuation of the vertical wind speed and acoustic temperature, and (2) a tethered balloon system (Vaisala TMT, Boulder), which was used for discontinuously profiling the ABL for air temperature, relative humidity, as well as mixing ratios of CO₂ and O₃. The meteorological sensor package of the tethered balloon system consisted of a thermistor for air temperature, a polymer based sensor for relative humidity, and a semiconductor technique based transducer for barometric pressure measurements. Wind speed (v_h) was measured by a 3-cup anemometer, and wind direction (ϕ) is determined by vane referring to an electronic compass. The CO₂ sonde was constructed around the GMP343 sensor (Carbocap, Vaisala), which uses a single-beam dual-wavelength NDIR technology. Data were stored in a small data logger every 2 s. The lightweight O₃ sonde, a development of the University New Hampshire, is based on single beam UV absorption (Talbot et al., 2006). Its data were internally stored to a memory and downloaded after the flight. Flights with the tethered balloon were performed only in the evening and morning hours. Around noon, turbulence became too strong for undisturbed measurements. Furthermore, for security reasons, the flights are generally limited to conditions of wind speeds less than 9 m s⁻¹. To avoid swinging payload, trace gas sondes were attached directly below the belly of the blimp-shaped balloon. Three meteorological sondes, each measuring wind speed and wind direction, air temperature, relative humidity and barometric pressure, were attached to the tether line with 5 m vertical spacing between each other. The uppermost sonde was located approximately 5 m below the belly of the balloon. Ground based measurements at BASE#2 site, used for referencing the balloon sensors, were stored as 5 min averages in a data logger. Data from the SODAR-RASS and tethered balloon were stored on a notebook and a personal computer, respectively.

5441

An additional forest station was located directly down slope of the TOP station, halfway to the village of Hohenpeissenberg. Its data of wind speed and wind direction were used to check, if air masses could have been transported very close to the ground toward the TOP station.

All parameters being measured at the four stations and being relevant for this paper are listed in Table 1. For practical reasons, both field sites at the foot of the mountain (BASE#1 and BASE#2) will be considered as the "BASE" (in contrast to TOP station).

2.3 Quality control

Data from all ground based measurements were checked for periods with erroneous data due to power failures and subsequent restarting procedures as well as for artificial trace gas peaks originating from farming and other agricultural management activities close by. Flux data were prepared for analysis by applying an established quality control scheme (Foken et al., 2004).

Profile data obtained by the SODAR-RASS system were quality controlled by using an internal quality code, provided by the SODAR-RASS system (METEK User handbook of SODAR/RASS, 2000). Subsequently, a despiking procedure was applied, based on the procedure published elsewhere (Vickers and Mahrt, 1997).

All deployed meteorological sondes were compared against the current data of the ground based system before flight (i.e. typically in the early morning and late afternoon). The parameters being compared were: air temperature, relative humidity and barometric pressure. Tethersonde flight data were quality controlled by cross checking all parameters, measured independently by the three meteorological sondes, for consistency. The altitude of the sonde was recalculated after each flight (ascent and descent) by comparing the barometric pressure readings from the sondes against the pressure of the ground based weather station. Drifts were distributed linearly over the preceding flight. As a last step, the corresponding altitude for each data point was calculated by stepwise solving the barometric altitude equation. After each pair of ascent and descent, the final height deviation from 0 (i.e. ground level), which is a result of

5442

the discrete computation, was distributed linearly over the preceding flight. CO₂ data were corrected for changing barometric pressure, a temperature correction was not applied, as the CO₂ and the O₃ sensor perform an online temperature correction (O₃ also pressure correction).

5 2.4 Computed parameters

Additional supporting parameters were derived from the measured quantities, such as measures for atmospheric stability. To assess the state of atmospheric stability, the dimensionless stability parameter $\zeta = z/L$ was used, where z is the height of measurement and L is the Obukhov length, calculated according to Eq. (1).

$$10 \quad L = - \frac{u_*^3}{\kappa \frac{g}{T_V} \frac{Q_{HB}}{\rho \cdot c_p}} \quad (1)$$

Here, u_* is the friction velocity, κ is the von-Kármán constant, g is the acceleration of gravity, T_V is the virtual air temperature, Q_{HB} is the buoyancy flux, ρ is the air density, and c_p is the specific heat of air at constant pressure. Usually, L is computed by using the sensible heat flux and air temperature. However, we explicitly used the buoyancy flux and the virtual temperature instead, as the high humidity is expected to play a major role in atmospheric stability in the morning hours, where we will focus on. From the equation of turbulent kinetic energy (see e.g. Stull, 1988) it follows, that for $\zeta < -1$ the buoyancy term is dominant compared to the shear term, which is a precondition for free convection.

20 The height of the convective boundary layer (CBL), was determined from SODAR-RASS data by applying (1) the parcel method to profiles of air temperature (Holzworth, 1967, 1964) and (2) a method described by Beyrich (1997) to profiles of backscatter intensity.

5443

2.5 Investigation of long-term (monitoring) measurements

A more than 5 yr long monitoring dataset (October 2000–December 2005), obtained at the TOP station, was investigated for the occurrence of O₃ drop events. This was done to get evidence whether the SALSA field observations were the result of an exceptional situation, or if similar events occur frequently at the Hohenpeissenberg Observatory. For that, an automated detection scheme has been developed and was applied to the time series of the O₃ mixing ratio (1 min resolution), featuring the following criteria: (1) a moving minimum was computed, comprising ± 180 min around the current value of the O₃ time series. The time of the actual occurrence of the minimum was taken as input data for subsequent filtering procedures. (2) To ensure a clear separation of O₃ minima, only detected minima with a temporal spacing of at least 60 min were kept further on. (3) Half drop values were computed by considering the detected minimum values and the median O₃ mixing ratios within 90 to 30 min before the minimum. (4) The onset detection of the O₃ drop event was done with a geometrical approach. For that, virtual lines were constructed from the point, where the rising flank of the O₃ drop reached its half drop value after the minimum to data points prior to the event. The data point in the time series, corresponding to the virtual line with most negative slope, was taken as first guess point of onset. The first local maximum of O₃ before this point was taken as final point of the onset of the O₃ drop event. A similar approach was used for determination of the end of the O₃ drop event, using the half event value at the falling flank of the O₃ drop, and a maximum positive slope criterion. These geometrical approaches were chosen, because the O₃ drops can also occur during changing background levels of O₃, making a detection based on fixed thresholds impossible. Furthermore, all events detected by this scheme were subsequently filtered: (1) the minimum had to be more than 5 ppb below the value at begin and end of the event; (2) the O₃ level at the end of the event had to be within $\pm 25\%$ and \pm standard deviation of the O₃ level before the event; (3) the relative O₃ drop had to exceed 10% of the previous O₃ level; (4) at the O₃ minimum, the corresponding value of the nitric oxide (NO) mixing ratio had to

5444

exceed its pre event level + standard deviation, and had to reach at least 0.5 ppb. The last criterion was introduced to limit the detection to O₃ drop events with characteristics similar to those observed during the SALSA campaign.

5 An index, whether or not a mesoscale circulation system called Alpine Pumping (see Lugauer and Winkler (2005); also described below) was active at a certain day, was computed by checking the South-North wind component (V). If it changed from positive values before 06:00 h to negative values after 12:00 h, while the total global radiation exceeded 20 MJ m⁻² at this day, Alpine Pumping was assumed to be active.

3 Results

10 This chapter is subdivided into five parts. First, a typical “event” course of O₃ mixing ratio at the TOP station in the morning hours is presented. Then we describe the general characteristics of all observed events during the SALSA campaign. Third, mean diurnal cycles of the flow characteristics for a subgroup of three events are presented. Fourth, we focus on the strongest event within this subgroup (as a case study) and describe
15 its peculiarities as observed at TOP station, within the ABL and at the BASE. Fifth, the frequency of O₃ mixing ratio drop at the TOP station is determined by inspecting a more than 5 yr dataset. All times and dates given in the following are Central European Time (CET=UT+1 h).

3.1 The O₃ drop event

20 On several days during the SALSA campaign, an eye-catching drop of O₃ mixing ratio at the TOP station has been observed. An example is shown in Fig. 2. Although not every observed event was as strong as that on 5 September 2005, they were always an eye-catching deviation from the expected (quasi constant) mixing ratio of O₃ at the TOP station. Further analyses revealed, that the O₃ events were associated with a
25 couple of other distinctive features, which will be presented in the following.

5445

3.2 General characteristics

A total number of six O₃ drop events were observed during the SALSA campaign (22 August 2005–23 September 2005). The event durations ranged from 10 to 118 min, defined as the span of time during which O₃ levels remained below the half drop value,
5 the observed O₃ drop intensities covered 23 to 80% of the initially present O₃. Characteristics of the O₃ drop events are summarized in Table 2.

No correlation was found between the event duration and its intensity. All event days had almost clear skies during the morning, except for 3 September 2005, when a considerable number of cumulus clouds were present. The irradiated shortwave energy,
10 from night until the onset of the event, ranged between 1.8 MJ m⁻² and 2.4 MJ m⁻², depending on the onset time and the presence of scattered clouds. Neither the event duration nor the O₃ decrease intensity correlated with the irradiated energy.

All of the observed events occurred at low wind speeds, in 5 cases there was a distinct wind speed minimum, lasting 2 to 3 h. In 3 cases, a sudden, jump like, change
15 of wind direction during the event has been observed. Wind direction before the event was around south, after the event wind came from north-eastern directions. Two other events were characterised by more or less stable wind directions around east, while the last event was accompanied by a continuously turning wind from east at midnight over south in the early morning to west at the time of the event and then continuing
20 over north to east again in the evening.

3.3 Mean characteristics

From the wind characteristics of the six observed O₃ events (Table 2), a group of three occurrences with more or less similar flow patterns can be discerned. These are the last three events observed during the experiment (5, 7 and 8 September 2005). For
25 this group, the mean diurnal course of the wind and the absolute range of values was computed. The latter demonstrates the quasi identical flow regime on all three days. Figure 3 shows the mean diurnal course of horizontal wind speed (v_H), its west-east

5446

and south-north components (U and V , respectively), and the degree of persistence (P) of the wind direction at any time of the day. The calculation of P is done according to Lugauer and Winkler (2005), following Eq. (2), where P is defined as the temporal vector mean of the horizontal wind speed divided by the temporal arithmetic mean of the horizontal wind speed at any time of the day.

$$P(t) = \frac{\sqrt{\overline{U(t)^2} + \overline{V(t)^2}}}{\overline{v_h(t)}} \quad (2)$$

A value for P of 1 indicates, that every day at that time the wind blew from the same direction, a value of 0 indicates, that at that time all wind directions occurred at the same frequency.

A distinct, absolute minimum of v_h (Fig. 3a) can be observed around 09:00 h to 11:00 h in the morning. Additionally, P (Fig. 3d) approaches its minimum at the same time, indicating highly variable wind directions during that period. The quasi reversal of the mean flow becomes especially visible in the vector component V (Fig. 3c), where a fast change from southerly directions (positive values) to northerly directions (negative values) is obvious around that time.

To get a closer insight into the processes being possibly active in the ABL at these days, we now focus on the day with the strongest occurrence of the O_3 drop at TOP station, namely the 5 September 2005. This event was selected, as all accompanying processes are expected to be best observable during the most intensive event.

3.4 5 September 2005: Case study

The 5 September 2005 was a clear, sunny and warm day. The global radiation R_g at TOP station (Fig. 4a), shows a nearly perfect bell-shaped curve in the absence of clouds. The air temperature at the TOP station (Fig. 4b) varied only slightly between night and day, being almost constant around 13°C at night and smoothly increasing

5447

to values around 21°C in the afternoon. The horizontal wind speed v_h at the mountain summit (Fig. 4c) decreased from higher night time values to a minimum around 09:00 h, while slightly increasing again from afternoon to evening. The wind direction (Fig. 4d) changed slowly from east to south during the night and early morning, until around 09:00 h a jump like change to easterly directions occurred. After 11:00 h, the wind direction remained around north-east. O_3 mixing ratio (Fig. 4e) was quasi constant during night within a range from 40 to 50 ppb. Together with the change of wind direction around 09:00 h it crashed down to 7 ppb and recovered during the following three hours. Coinciding, NO mixing ratios increased from below the detection limit to 12 ppb and decreased during the following hours (Fig. 4f).

The presence of SODAR-RASS and tethered balloon systems provided the unique chance of observing the state of the ABL up to well above the mountain summit with respect to wind, turbulence, air temperature and the trace gases CO_2 , O_3 and H_2O . Figure 5 presents time-height cross sections of wind direction ϕ (Fig. 5a), horizontal wind speed v_h (Fig. 5b) and potential air temperature θ (Fig. 5c), all for the interval from 4 September, 21:00 h to 5 September 2005, 15:00 h.

In the lowest 130 m, a layer with westerly winds developed during the night (Fig. 5a), beginning around 23:00 h in the evening. The different wind direction within this layer (compared to the layer above) indicated that it was completely decoupled from the air above. The lower layer was the nocturnal boundary layer, while the upper one was the residual layer. The nocturnal boundary layer reached its maximum vertical extent shortly after 03:00 h in the morning. At this time, wind direction changed also in higher altitudes from easterly to southerly directions. A distinct spatial boundary with respect to directional wind shear, was no longer observable from this time on. After sunrise around 06:00 h, the entire observable ABL was characterized by a smooth transition from westerly winds close to the ground to southerly wind directions above 300 m a.g.l. Shortly after 08:00 h, the wind changed abruptly to easterly directions. This change affected all levels in the lowest 200 m at the same time, while the change was gradually delayed at higher altitudes.

5448

Coinciding with the change of wind direction, the horizontal wind speed (Fig. 5b) dropped to very low values ($<1 \text{ ms}^{-1}$). These low wind speeds prevailed only shortly in the lowest 200 m of the atmosphere, being followed by stronger fluctuations with peak values of approx. 4 ms^{-1} . Above 200 m a.g.l., the calm period lasted considerably longer and the onset of the fluctuations was delayed by approximately two hours. The last parameter of the SODAR-RASS system considered here is the potential air temperature θ (Fig. 5c). Starting in the late evening, a very stable thermal stratification of the ABL developed by radiative cooling of the surface. A gradual increase of θ in the entire profile was interrupted around 09:00 h by a temperature drop. It became first visible close to the ground, but affected the entire observable atmosphere within half an hour. After that, the ongoing solar heating of the ground led to the development of a thermally unstable ABL.

The height of the boundary layer BL (z_{BL}) was determined from 15 min average profiles of θ using the parcel method (Holzworth, 1967, 1964) and from half-hourly average profiles of the reflectivity of the vertical acoustical antenna by visual inspection, whereas a secondary maximum of reflectivity indicates the BL height (Beyrich, 1997). Both methods yielded similar BL heights (Fig. 6) with a maximum of 380 m at 13:30 h. The onset of the evolution of the convective boundary layer CBL detected by the parcel method (09:00 h) was one hour later than inferred from the reflectivity data (08:00 h). Growth rates of the CBL were around 50 m h^{-1} with both methods. The height of the CBL reached the TOP station around 12:00 h, that means, the TOP station was clearly outside the CBL around 09:00 h.

Besides the profiles with high temporal resolution obtained by the SODAR-RASS system, profile data from the tethered balloon system were available for the morning hours of 5 September 2005. The system was operated in scanning mode, i.e. the profiles were obtained by raising and lowering the balloon continuously. Scanning mode provides a good spatial resolution but with some temporal ambiguity in the profiles, resulting from the time needed for a complete scan. The main advantage of the tethered balloon system was its ability to measure profiles of the trace gases CO_2 , O_3

5449

and the specific humidity q besides the meteorological data. However, trace gas data add invaluable information to the profiles obtained by the SODAR-RASS system. By chance, one of these scanned profiles at 5 September 2005 captured the event and gave insight into its vertical structure. A set of time-height cross sections and profiles for q , O_3 , CO_2 and θ are shown in Fig. 7. The time-height cross sections of q , O_3 , CO_2 and θ (Fig. 7a–d) show a growing but clearly confined layer of higher q and CO_2 and lower O_3 and θ compared to the air above from about 07:30 h. After 09:30 h, in the last descent of the tethered balloon, this confinement is no longer visible. In Fig. 7d (θ), a pool of cold, nocturnal air close to the ground can be identified. Between 07:00 h and 08:00 h, this surface air rapidly warms up, but still remains colder than the air aloft.

The profiles on the right side of Fig. 7 depict the upward scan of the tethered balloon at the time of the O_3 drop at TOP station. All profiles can be divided into the following segments: (1) a lower part up to 130 m a.g.l. with almost constant values for all parameters, capped by a temperature inversion (Fig. 7d), which results in a drop of q and also of CO_2 , whereas O_3 starts to increase from this altitude on (this layer coincides very well with the CBL determined from the SODAR-RASS data); (2) at 290 m a.g.l., a distinct layer of approx. 30 m thickness becomes obvious, being characterized by enhanced water content, higher CO_2 values and by a reduced O_3 level; (3) at the top of the profiles at 420 m a.g.l., the trace gases CO_2 and O_3 reached typical lower tropospheric background levels of 360 ppm and 50 ppb, respectively, while q reached approx. 6.5 g kg^{-1} .

After the temporal and spatial changes within the ABL have been described in detail, the observations at the BASE will be examined.

The characteristics of the wind at the BASE with respect to speed and direction were comparable to that within the ABL, especially the sudden change of the flow direction around 09:00 h (see Fig. 8c,d). Following the cold night, the sensible heat flux started to increase shortly after sunrise (Fig. 8a) together with increasing air temperature (Fig. 8b). With the onset of the event, a clear drop of air temperature was observed, lasting for almost one hour. The time of the temperature decrease coincided

5450

well with temperature decrease of the entire ABL, observed by the SODAR-RASS system (Fig. 5c). The stability parameter ζ (Fig. 8e), being valid for the surface layer, showed mostly positive values during night, indicating stable conditions. But with H around 0, values of ζ were of low quality and must be used very carefully. The most
5 unstable situation within the surface layer was found around 08:30 h, where ζ reached values of -1.2 . Later towards noon, unstable conditions prevailed ($\zeta \approx -0.3$). Friction velocity u_* (Fig. 8f) was slightly increasing from its night time values ($\approx 0 \text{ m s}^{-1}$), and reached only small secondary minimum values ($\approx 0.1 \text{ m s}^{-1}$) at 09:00 h. With the increasing buoyancy due to increasing sensible heat flux, and the decreasing shear,
10 indicated by low u_* values, this forms the conditions needed for free convection (Stull, 1988). O_3 mixing ratio decreased during night at the BASE to zero (not shown here). With increasing insolation and developing turbulence, it started to increase until shortly before 09:00 h, when a drop back to the low nocturnal values occurred. The later increase of O_3 mixing ratio was again interrupted around 10:30 h, when O_3 mixing ratio
15 remained for approximately two hours at a more or less constant level.

3.5 Long dataset

After the detailed description of the observations coinciding with the O_3 drop at TOP station, within the ABL, and at the BASE, we evaluated a 5 yr dataset (October 2000 to December 2005) of the TOP station for the occurrence of sudden O_3 decreases.
20 As the events observed during the SALSA experiment were restricted to days with high irradiation, we split the analysis into days with total irradiated energy exceeding 20 MJ m^{-2} and days with less energy input. The radiation days were further subdivided into days with and without Alpine Pumping. The resulting diurnal histogram is shown in Fig. 9. The class with low radiation shows a smooth distribution curve, with highest
25 values between 08:00 h and 10:00 h. During night, only few events were detected. Both classes with high irradiated energy are characterized by a sharp peak in the early morning, with maximum frequency between 08:00 h and 09:00 h. In the afternoon and during night, there were almost no events found.

5451

4 Discussion

At a first glance, several explanations for the O_3 drop events seem to be possible from our observations. “Transport” is common to all of them, however varying in important aspects. It is known from earlier studies (Lugauer and Winkler, 2005), that the region
5 of the SALSA experiment is occasionally affected by a mesoscale circulation system between the Alps and their northern foreland (Alpine Pumping). Whether or not this circulation was present during the experiment and whether it impacts the observations will be discussed in the first section.

The variability of the O_3 drop intensity, its peak time and its event duration (see Table 2) suggest highly dynamical processes behind this phenomenon. A number of processes leading to the observed O_3 drop events are conceivable: (1) a local, temporally limited O_3 sink close to mountain summit, (2) a local valley to mountain circulation, including the influence from a national road passing the foot of the mountain in east-west
10 direction, (3) change of air masses (passage of fronts), (4) immersion of the mountain summit into the developing convective boundary layer, and (5) direct injection of air masses by free convection from the foot of the mountain into higher ABL altitudes. From the observations presented in the results chapter, we will demonstrate that it is possible to narrow the number of these processes down to one final explanation: free convection. For that, after a brief description of the mesoscale circulation system
15 “Alpine Pumping”, we will start with the most local process and will increase the spatial dimension step by step.

4.1 Mesoscale circulation system – Alpine Pumping

On days of high solar irradiance, barometric pressure in the valleys of the Alps becomes low relative to the Alpine foreland due to enhanced heating up of the valley air.
25 This horizontal pressure difference forces air during day time to flow from the foreland plains towards the Alps mountains, where it rises convectively. The diurnal counter flow from mountain to foreland occurs in higher altitudes. For dynamical reasons, it

5452

causes a subsidence over the foreland with typically cloud free skies. During night time, stronger cooling in the valleys leads to higher barometric pressure in the valleys, resulting in an outflow of air towards the foreland plains (Whiteman and Bian, 1998, 2000).

5 The influence of thermally driven wind systems in the area of the SALSA experiment, was intensively investigated by Lugauer and Winkler (2005). The diurnal oscillation of the wind direction, caused by the heating and cooling of the Alps, was found to affect the Alpine foreland up to 100 km to the north with a vertical extent of 1 km at the Alpine margin. From 340 days with strong irradiation (out of 5 yr), Lugauer and Winkler
10 (2005) calculated mean diurnal cycles of horizontal wind speed, west-east and south-north wind components and the persistence of wind direction at the Hohenpeissenberg summit.

The comparison of the mean diurnal cycles from Lugauer and Winkler (2005) with mean diurnal cycles from the SALSA experiment (Fig. 3), reveals a striking similarity,
15 although our results are only based on 3 days. Nevertheless, for these 3 days, we can assume that a similar flow regime, the Alpine Pumping, was dominating the experimental site. Additionally, in accordance with Lugauer and Winkler (2005), Fig. 5a shows a slight delay of the wind direction change in higher altitudes compared to the surface layer, caused by the typical speed at which this circulation system develops.

20 A fast change of wind direction, especially when it comes close to a flow reversal, always implies a period of low to zero wind speed. With the Alpine Pumping starting to affect the TOP station (indicated by the South-North wind component (V) changing from positive to negative values), such calm situations were associated. They lasted from some minutes up to more than half an hour. This is noteworthy, as low horizontal
25 wind speeds can trigger some of the processes discussed in the following (i.e. free convection).

5453

4.2 Local sink for O₃ at mountain summit

Strong local sinks for O₃ within 300 m to the TOP station, which could facilitate a substantial drop of O₃ mixing ratio at the TOP station, can be excluded. Adverse effects of the station itself (exhaust from lab vents etc.) are not likely, since the setup of the
5 observatory as a background trace gas measurements station of Global Atmosphere Watch (GAW) program has to follow corresponding operational guidelines. In the unlikely case, that some exhaust gas from cars from the parking lot at Hohenpeissenberg summit would have reached the gas sampling inlet, it would have resulted in a sharp but short O₃ drop rather than in an O₃ breakdown lasting half an hour and more. Further-
10 more, this would happen only in the case of (local) wind directions around 90°–100°. However, the mean annual frequency of these wind directions is less than 5%. On 5 September 2005, the mean wind direction at the time of the onset of the O₃ drop event was from South, so the parking lot was not upwind of the TOP station.

After the explanation that there are no sources of O₃ destruction at the mountain
15 summit, we will now focus on the area south of the mountain summit because, as concluded from the wind direction, the reason for the O₃ drop must be located there.

4.3 Valley to mountain circulation system

The high frequency of O₃ drop events in the morning hours may point to a local, thermally driven, valley to mountain circulation at Hohenpeissenberg mountain. The high
20 solar irradiance and the partly deforested slope of the mountain would support this idea. Furthermore, the village of Hohenpeissenberg is located at the lower end of the deforested south flank of the mountain, and a national road passes by. Together, village and road would provide enough O₃ destructors (mainly NO from heating and exhaust gases). But although this mechanism might seem to be the most probable one, several
25 results of our measurements point into a different direction.

First, at the SALSA forest station at the southern slope of the mountain, half way between the deforested area and the summit, the wind direction remained around North,

5454

which is a downhill flow, at mean wind speeds around 0.5 m s^{-1} . From that, an upslope wind, at least in the trunk space of the forest, can be excluded.

Second, one of the vertical scans of the tethered balloon (Fig. 7, right panel) hit an O_3 poor layer at approx. 300 m a.g.l. at 5 September 2005, 09:16 h, which is shortly after the maximum intensity of the O_3 drop at the TOP station. The tethered balloon profiles were measured in a horizontal distance of approx. 1.6 km from the TOP station (as referenced to the launching site of the balloon). Even with some northward drift of the balloon due to the southerly winds, the O_3 poor air mass was detected still more than 1 km south of the summit. The wind direction from south makes it impossible for an air mass being upslope transported by a valley to mountain circulation to be found 1 km south of the mountain summit. Under the assumption, that the O_3 poor air mass observed by the balloon is in coherence with the O_3 event at the TOP station, which will be proven below, a local valley to mountain circulation has to be definitely excluded as the dominating process.

4.4 Airmass change, passage of fronts

The sudden drop of O_3 mixing ratio at the TOP station, together with the change of wind direction, could suggest a change of air masses. But in this case, O_3 values would have to stay low after the event and would not recover to values comparable to those before. Additionally, a peak in NO would not be expected, as NO must have been transported very fast towards the TOP site to not be converted into NO_2 due to reaction with the present O_3 during the transport. But after the O_3 drop event, comparable levels of O_3 mixing ratio have been observed, and NO (Fig. 4f) as well as NO_2 (not shown) dropped back to its pre event values close to 0. This indicates, that only a temporal excursion from the state prior to the event had occurred and not a general change. Furthermore, the sharp boundaries of the O_3 depleted layer observed by the tethered balloon (Fig. 7b) suggest only a short transport time. Longer lasting transport would have smeared out the boundaries due to turbulent diffusion. Based on that,

5455

advection from greater distance, embedded in a different air mass, becomes highly unlikely. Around the O_3 drop event, a slight cooling of the entire ABL was observable (Fig. 5c), although the irradiation remained undisturbed (Fig. 4a). As concurrency is always conspicuous, and an air mass change can be excluded, an independent explanation for the cooling has to be found, preferably a process, comprising the cooling and the simultaneous presence of the O_3 depleted layer. This could provide a proper explanation of the dynamics behind the O_3 drop events. But before such an attempt will be made, other processes being relevant in the morning hours have to be examined (and finally excluded).

4.5 Immersion of TOP station into CBL

The altitude of the wind direction change (Fig. 5a) did not coincide with the height of the CBL at this time. Although the CBL growth started at the same time as the wind direction started to change at the BASE, its height was still about 150 m less than the altitude of the layer affected by wind direction change. In Fig. 5b, the CBL can be identified as the region of enhanced wind speed fluctuations, reaching values of around 5 ms^{-1} in the afternoon. An independent confirmation is given by Fig. 6, where the CBL height is derived from the profile of θ , which gives the height up to which an air parcel may rise by buoyancy if released at ground, as well as the CBL height derived by visual inspection of the reflectivity data. Compared to other fair weather days during the experiment (not shown here) the evolution of the CBL started late, the growth rate was much lower and the CBL height reached a very low maximum height. Growth rates of $100 \dots 1000 \text{ m h}^{-1}$ (Seibert et al., 1998) are reported and maximum heights of the CBL on the order of 1 to 2 km (Stull, 1988) are expected on clear, sunny days over terrestrial surfaces in mid latitudes. The lateral heterogeneity of the land, with patches contributing more (grassland, villages) or less (forest, rivers, lakes) to the development of the CBL reduces the expected growth rates and maximum height around the SALSA site. Furthermore, subsidence over the Alpine foreland, as a result of Alpine Pumping (Lugauer and Winkler, 2005), suppresses the CBL growth even

5456

more. The combination of both processes led to a height of the CBL well below the summit of the Hohenpeissenberg mountain at the time of the O₃ drop event. Immersion of the mountain summit into the developing CBL can thus be definitely excluded as explanation.

5 4.6 Convective injection of surface layer air into higher ABL levels

The highly unstable conditions within the surface layer in the morning hours of 5 September 2005 suggested additional consideration of convective processes as a reason for the development of the O₃ poor layer within the ABL. With positive sensible heat flux (see Fig. 8a), a shallow but forced convection was established shortly after sunrise (06:00 h), initiating the development of a CBL. Increasing sensible heat flux and a simultaneously occurring secondary minimum of u_* led to a dominance of buoyancy created turbulence over shear created turbulence (see Eq. (1)), – a state of free convection. Somewhere, upwind of the mountain, warm air masses, already heated up for several hours, became sufficiently buoyant and rose in a pulse-like motion up to its equilibrium height. As the air close to the ground was still poor of O₃ but rich in CO₂ and H₂O, a small layer with lower O₃ and higher CO₂ and H₂O (compared to the surrounding air) developed. Together with the surrounding air mass (which was still statically stable), it was horizontally advected towards the mountain. Recalling Fig. 5b, the wind speed at mountain summit remained at very low values for some hours. This explains, why the event duration at 5 September was quite long with a very slow recovery of the O₃ values afterwards.

Two independent confirmations for such a process can be found in the dataset.

(1) The drop of air temperature (Fig. 8b), (not shown: simultaneous drop of H₂O and O₃ and increase of CO₂) at the BASE shortly before the onset of the O₃ decrease at the TOP station (see Fig. 4e). Again, the temporal concurrency of these observations with the TOP station observations suggests a common process. The air mass, being lifted by free convection in the surrounding of the BASE, had to be

5457

replaced by another air mass. This replacement air originated most probably from the trunk space of the forest, encompassing the BASE from east to southwest. Despite strong irradiance, the air in the trunk space was still relatively cold (air temperature drop), less affected by photochemistry than the air in the open surrounding of the BASE, and due to little vertical transport through the forest canopy still enriched in CO₂, a remainder from the night time respiration of soil and plants.

(2) A simple backward trajectory estimate confirmed, that the source region of the convectively lifted air mass should have been at the southern part of the village Hohenpeissenberg, approx. 500 m northwest of the BASE (Fig. 10). For this estimate, some assumptions had to be made. First, the wind field was assumed to be horizontally homogeneous in all heights. This is a rough estimation, especially at low wind speeds, but for our purpose this approximation can be done. With that, the wind vector at every time of the calculation was taken from the respective height of the SODAR wind profiles. Second, the convective vertical transport was assumed to be constant at approx. 1.5 ms⁻¹ during the ascent from the surface to 288 m a.g.l. This is in accordance with textbook values for the convective velocity scale around 09:00 h in the morning (Stull, 1988). A direct calculation of the convective velocity scale from available data seemed to be inappropriate, as the described process must have been considerably stronger than the convective velocity within the still relatively shallow CBL.

According to reasonings (1) and (2), the phenomenon of O₃ drop events at the mountain summit is thus a combination of a free convective pulse in the morning and a subsequent advection process transporting this air parcel towards the TOP station. The trigger of the free convective pulse can either be the wind speed minimum or just a sufficient energy input by solar radiation under low wind conditions. Whether the wind speed drops due to the onset of Alpine Pumping or is just ceasing due to the synoptical

5458

situation will not affect the development of an unstable condition and thus the release of a convective pulse. Furthermore, the observation of a wind speed minimum leading to a free convective pulse is subject to some luck, as convective cells are known to have a very limited horizontal dimension (Shen and Leclerc, 1997). On 5 September 2005 we had the luck to measure within or close by such a cell. Nevertheless, convective cells can certainly develop without us being able to observe them in our ground based measurements. This explains, why some of the events listed in Table 2 are apparently not associated with a distinct wind speed minimum. The discrimination of O₃ drop events at TOP site, as a result of a pulse of free convection, from other causes is thus the main challenge of evaluating a long time series of O₃ measurements at the TOP station for the occurrence of O₃ drop events with a similar causation as the events described in this paper.

4.7 Long dataset

Starting with one day (5 September 2005), where all observations were made just at the right place and time, and expanding the findings to a more than 5 yr period, requires a critical limitation of possible statements. One of these limitations is a clear assignment of observed events to certain processes. The diurnal distribution of O₃ drop event frequencies (Fig. 9) shows a clear difference between days with high global radiation and low global radiation. In the latter case, O₃ drop events were distributed as a diurnal cycle over day times, with a weak maximum between 09:00 h and 10:00 h (Fig. 9, black bars). In contrast, for days with high global radiation, O₃ drop event frequencies sharply peaked between 07:00 h and 09:00 h (Fig. 9, grey bars) and events were restricted to the morning hours. This gives evidence of a process, being restricted to high energy input and being primarily present in the early morning hours. As described in Sect. 4.1., the independent phenomenon of Alpine Pumping is also bound to high global radiation days. It is able to provide a (secondary) wind speed minimum in the morning hours. From that we can make two statements: (a) due to Alpine Pumping, conditions favourable for free convection occur frequently in early morning hours of

5459

fair weather days, and (b) on fair weather days we observed maximum frequency of O₃ drop events at the TOP station. Together, this clearly points towards a convective pulse, as it was discussed in the previous section. Almost half of the events with high energy input (84 events) occurred at days, when the mesoscale circulation Alpine Pumping occurred. We found Alpine Pumping to occur at 46% of all days during which total global radiation exceeded 20 MJ m⁻². This is in excellent agreement with Lugauer and Winkler (2005), who found 42%. The onset of the circulation, with its associated change of wind direction, must cause a short minimum of horizontal wind speed. Again, this points to a convective process, as low wind speeds are known to increase already present thermal instability. The other half of the events with high energy input (85 events) was not connected to Alpine Pumping. At least, characteristics of Alpine Pumping were not observable at the TOP station at these days. But horizontal wind speed is generally not very high during fair weather days, and can furthermore drop to low values for various reasons – leading to the same destabilisation of moist and heated air masses.

Daily total global radiation of more than 20 MJ m⁻² is in midlatitudes restricted to a period approx. from April to September. During this period, the TOP site was in 18% of the days affected by an O₃ drop event, coupled to high energy input, being most probably the result of a convective pulse. Half of those events are even more likely to originate from a free convective pulse, as they occurred at days with Alpine Pumping, where a short wind speed drop in the morning hours occurs. Furthermore, these numbers have to be taken as a minimum estimation, as the convectively lifted air masses have not necessarily to be advected towards the TOP site or have to be trapped just at the right altitude to hit the TOP station.

5 Conclusions

The observed O₃ drop events result from free convection in the morning hours, having the power to rise far above the height of the growing CBL. The trigger of the convection

5460

can be manifold and are not necessarily limited to a mesoscale circulation system as it was the case in half of the days in this study. The described processes provide a powerful vertical transport mechanism in the early morning hours, which has a strong impact on atmospheric chemistry (trace gases) and meteorology (air temperature) close to ground as well as in higher altitudes.

The O₃ drop events were not only observed during the field experiment but were present throughout the entire period from October 2000 to December 2005. At 18% of the days between April and September, the O₃ decreases are most likely the result of a free convective pulse in the early morning.

It can be expected, that similar processes are active also in other regions, where appropriate triggers like local or mesoscale circulation systems lead to a convective release of surface layer air masses into the residual layer. Whether or not such transport events are sufficiently captured by common flux measurement techniques should be carefully investigated. This becomes particular true, when observed trace gas concentrations are to be assigned to possible source regions, only based on the wind direction.

Acknowledgements. The authors are grateful to all people supporting the field measurements, especially the staff of the Bauhof Hohenpeissenberg and families Schindler, Graf and Wiedemann. Special thanks belong to the German Meteorological Service and the staff of its observatory Hohenpeissenberg for performing additional measurements and providing data. The project was funded by Max Planck Society and German Science Foundation (DFG).

References

- Aneja, V. P., Arya, S. P., Li, Y., Murray, G. C., JR., and Manuszak, T. L.: Climatology of Diurnal Trends and Vertical Distribution of Ozone in the Atmospheric Boundary Layer in Urban North Carolina, *J. Air Waste Manage.*, 50, 54–64, 2000.
- Attmannspacher, W. and Hartmannsgruber, R.: On Extremely High Values of Ozone Near the Ground, *Pure Appl. Geophys.*, 106–108, 1091–1096, 1973.

5461

- Beyrich, F., Weisensee, U., Sprung, D., and Güsten, H.: Comparative analysis of sodar and ozone profile measurements in a complex structured boundary layer and implications for mixing height estimation, *Bound.-Lay. Meteorol.*, 81, 1–9, 1996.
- Beyrich, F.: Mixing Height Estimation from SODAR Data – a Critical Discussion, *Atmos. Environ.*, 31, 3941–3953, 1997.
- Cheng, W.-L.: A vertical profile of Ozone concentration in the atmospheric boundary layer over central Taiwan, *Meteorol. Atmos. Phys.*, 75, 251–258, 2000.
- Corsmeier, U., Kalthoff, N., Kolle, O., Kotzian, M., and Fiedler, F.: Ozone concentration jump in the stable nocturnal boundary layer during a LLJ-event, *Atmos. Environ.*, 31, 1977–1989, 1997.
- Fast, J. D., Doran, J. C., Shaw, W. J., Coulter, R. L., and Martin, T. J.: The evolution of the boundary layer and its effect on air chemistry in the Phoenix area, *J. Geophys. Res.-Atmospheres*, 105, 22 833–22 848, 2000.
- Foken, T., Göckede, M., Mauder, M., Mahrt, L., Amiro, B. D., and Munger, J. W.: Post-field data quality control, in: *Handbook of Micrometeorology: A Guide for Surface Flux Measurements*, edited by: X. L., Kluwer, Dordrecht, 81–108, 2004.
- Güsten, H., Heinrich, G., and Sprung, D.: Nocturnal depletion of ozone in the Upper Rhine Valley, *Atmos. Environ.*, 32, 1195–1202, 1998.
- Hastie, D. R., Narayan, J., Schiller, C., Niki, H., Shepson, P. B., Sills, D. M. L., Taylor, P. A., Moroz, W. J., Drummond, J. W., Reid, N., Taylor, R., Roussel, P. B., and Melo, O. T.: Observational evidence for the impact of the lake breeze circulation on ozone concentrations in Southern Ontario, *Atmos. Environ.*, 33, 323–335, 1999.
- Holzworth, C. G.: Estimates of Mean Maximum Mixing Depths in the Contiguous United States, *Mon. Weather Rev.*, 92, 235–242, 1964.
- Holzworth, C. G.: Mixing depths, wind speeds, and air pollution potential for selected locations in the United States, *J. Appl. Meteorol.*, 6, 1039–1044, 1967.
- Lee, S.-M., Fernando, H. J. S., Princevac, M., Zajic, D., Sinesi, M., McCulley, J. L., and Anderson, J.: Transport and Diffusion of Ozone in the Nocturnal and Morning Planetary Boundary Layer of the Phoenix Valley, *Environ. Fluid Mech.*, 3, 331–362, 2003.
- Lin, C.-H., Wu, Y.-L., Lai, C.-H., Lin, P.-H., Lai, H.-C., and Lin, P.-L.: Experimental investigation of ozone accumulation overnight during a wintertime ozone episode in south Taiwan, *Atmos. Environ.*, 38, 4267–4278, 2004.
- Lugauer, M., and Winkler, P.: Thermal circulation in South Bavaria – climatology and synoptic

5462

- aspects, *Meteorol. Z.*, 14, 15–30, 2005.
- McKendry, I. G., Steyn, D. G., Lundgren, J., Hoff, R. M., Strapp, W., Anlauf, K., Froude, F., Martin, J. B., Banta, R. M., and Olivier, L. D.: Elevated ozone layers and vertical down-mixing over the Lower Fraser Valley, bc, *Atmos. Environ.*, 31, 2135–2146, 1997.
- 5 McKendry, I. G., Steyn, D. G., O’Kane, S., Zawar-Reza, P., and Heuff, D.: Lower Tropospheric Ozone Measurements by Light Aircraft Equipped with Chemiluminescent Sonde, *J. Atmos. Ocean. Tech.*, 15, 136–143, 1998.
- Müller, H. and Sladkovic, R.: Case Studies of Frontal Passages in a Mountain Valley with Direct Access to the Bavarian Pre-Alpine Region Results from the German Front Experiment 1987, *Meteorol. Atmos. Phys.*, 43, 77–87, 1990.
- 10 Prévôt, A. S. H., Dommen, J., Bäumle, M., and Furger, M.: Diurnal variations of volatile organic compounds and local circulation systems in an Alpine valley, *Atmos. Environ.*, 34, 1413–1423, 2000.
- Reitebuch, O., Strassburger, A., Emeis, S., and Kuttler, W.: Nocturnal secondary ozone concentration maxima analysed by sodar observations and surface measurements, *Atmos. Environ.*, 34, 4315–4329, 2000.
- 15 Rummel, U.: Turbulent exchange of ozone and nitrogen oxides between an Amazonian rain forest and the atmosphere, University of Bayreuth, Bayreuth, 2005.
- Salmond, J. A. and McKendry, I. G.: Secondary ozone maxima in a very stable nocturnal boundary layer: Observations from the Lower Fraser Valley, BC, *Atmos. Environ.*, 36, 5771–5782, 2002.
- 20 Seibert, P., Beyrich, F., Gryning, S. E., Joffre, S., Rasmussen, A., and Tercier, P.: Mixing layer depth determination for dispersion modeling, in: COST Action 710-Final Report. Harmonisation of the pre-processing of meteorological data for atmospheric dispersion models, edited by: Fisher, B. E. A., Erbrink, J. J., Finardi, S., Jeannot, P., and Thomson, D. J., European Commission, 2985 Luxembourg, 431, 145–265, 1998.
- Shen, S. and Leclerc, M. Y.: Modelling the turbulence structure in the canopy layer, *Physical and Biophysical Processes in the Vegetation, Environment*, 87, 3–25, 1997.
- Strong, C., Fuentes, J. D., Davies, R. E., and Bottenheim, J. W.: Thermodynamic attributes of Arctic boundary layer ozone depletion, *Atmos. Environ.*, 36, 2641–2652, 2002.
- 30 Stull, R. B.: An introduction to boundary layer meteorology, Kluwer Academic Publisher, Dordrecht, 666 pp., 1988.
- Talbot, R., Mao, H., Troop, D., Moore, B., Johnson, R., and Businger, S.: Smart balloon ob-

5463

- servations over the North Atlantic: Part I – Mini-O3 sampling of urban plumes, *J. Geophys. Res.*, 111, D23S56, doi:10.1029/2005JD006507, 2006.
- Vickers, D. and Mahrt, L.: Quality Control and Flux Sampling Problems for Tower and Aircraft Data, *J. Atmos. Ocean. Tech.*, 14, 512–526, 1997.
- 5 Wanner, H., Künzle, T., Neu, U., Ihly, B., Baumbach, G., and Steisslinger, B.: On the Dynamics of Photochemical Smog over the Swiss Middleland – Results of the First POLLUMET Field Experiment, *Meteorol. Atmos. Phys.*, 51, 117–138, 1993.
- Whiteman, C. D. and Bian, X.: Use of Radar profiler data to investigate large-scale thermally driven flows into the Rocky Mountains, 4th Int. Symp. trop. Profiling, Snowmass, CO, 329–331, 1998.
- 10 Whiteman, C. D. and Bian, X.: Mountain Meteorology, Oxford University Press, 355 pp., 2000.
- Yelansky, N. F. and Senik, I. A.: Measurements of surface ozone concentrations at the high-mountain scientific station Kislovodsk: The seasonal and daily variations, *Atmospheric and Oceanic Physics*, 31, 235–243, 1995.
- 15

5464

Table 1. Measured parameters at the TOP station, forest station and the two sites of the BASE.

Parameter	Symbol	Unit	Temporal resolution (min)	Sampling height (m) a.g.l.	Instrument (Model)
TOP station, 998 m above sea level					
Air temperature	T	$^{\circ}\text{C}$	1	2	PT100
Relative Humidity	rH	%	1	2	LI-CI-Sensor, Rotronic
Air pressure	P	hPa	1	2	
Horizontal wind speed	v_h	ms^{-1}	1	40.5	Cup anemometer, heated
Wind direction	ϕ	$^{\circ}$	1	40.5	Vane, heated
Global radiation	R_g	Wm^{-2}	1	18	CM11, Kipp&Zonen
Ozone	O_3	ppb	1	18	UV absorption; ThermoElectron, 49C
Nitric oxide	NO	ppb	1	18	Chemiluminescence; ECO Physics CLD 770 AL ppt
Nitrogen dioxide	NO_2	ppb	1	18	ECO Physics CLD 770 AL ppt with PLC 760
Carbon monoxide	CO	ppb	1	18	Resonance fluorescence; Aero Laser AL 5001
BASE#1 station, 735 m above sea level, flux site					
Sensible heat flux	H	Wm^{-2}	30	2	Campbell CSAT3
Friction velocity	u_*	ms^{-1}	30	2	Campbell CSAT3
BASE#2 station, 710 m above sea level, sounding site					
Air temperature	T	$^{\circ}\text{C}$	5	2	Rotronic
Relative humidity	rH	%	5	2	Rotronic
Air pressure	P	hPa	5	1	Vaisala, PTB101B
Horizontal wind speed	v_h	ms^{-1}	5	2	Vector instruments
Wind direction	ϕ	$^{\circ}$	5	2	Vector instruments
Ozone	O_3	ppb	5	3.5	ThermoElectron, 49C
Nitric oxide	NO	ppb	5	3.5	TECAN 700 AL
Nitrogen dioxide	NO_2	ppb	5	3.5	TECAN 700 AL
Carbon dioxide	CO_2	ppm	5	3.5	LiCor 840
Water vapour	H_2O	ppth	5	3.5	LiCor 840
Acoustic temperature	\bar{T}_a	$^{\circ}\text{C}$	5	40–450	RASS, METEK
Horizontal wind speed	v_h	ms^{-1}	5	40–450	SODAR, METEK
Wind direction	ϕ	$^{\circ}$	5	40–450	SODAR, METEK
Reflectivity	R	dB	5	40–450	SODAR, METEK
Air temperature	T	$^{\circ}\text{C}$	Approx. 30	1–450	Tethered balloon, TMT, Vaisala
Relative humidity	rH	%	Approx. 30	1–450	Tethered balloon, TMT, Vaisala
Air pressure	P	hPa	Approx. 30	1–450	Tethered balloon, TMT, Vaisala
Forest station, 850 m above sea level					
Horizontal wind speed	v_h	ms^{-1}	5	2	Vector instruments
Wind direction	ϕ	$^{\circ}$	5	2	Vector instruments

5465

Table 2. Characteristics of O_3 drop events. Event durations are defined as the span of time during which the O_3 level remains below 50% of maximum drop intensity (full width of half event maximum). Minimum O_3 shows the O_3 mixing ratio at event maximum, the relative O_3 decrease gives the percentage of initially present O_3 being missed during the event.

	30 Aug	31 Aug	3 Sep	5 Sep	7 Sep	8 Sep
Onset time (CET)	08:00	09:00	08:15	08:30	09:15	09:30
Peak time (CET)	08:30	10:30	08:54	09:05	09:48	09:50
Duration (min)	13	71	27	118	15	10
Initial O_3 level (ppb)	45	45	48	41	46	48
Minimum O_3 level (ppb)	27	20	22	7	19	37
Relative O_3 decrease (%)	40	56	54	81	59	23
ϕ before event ($^{\circ}$)	90	180	90	180	180	180
ϕ after event ($^{\circ}$)	50	360	30	45	45	50
v_h minimum observed?	Yes	No	Yes	Yes	Yes	Yes
Type ϕ change	constant	Transition at low rates	Fluctuating but constant	jump like	jump like	jump like

5466

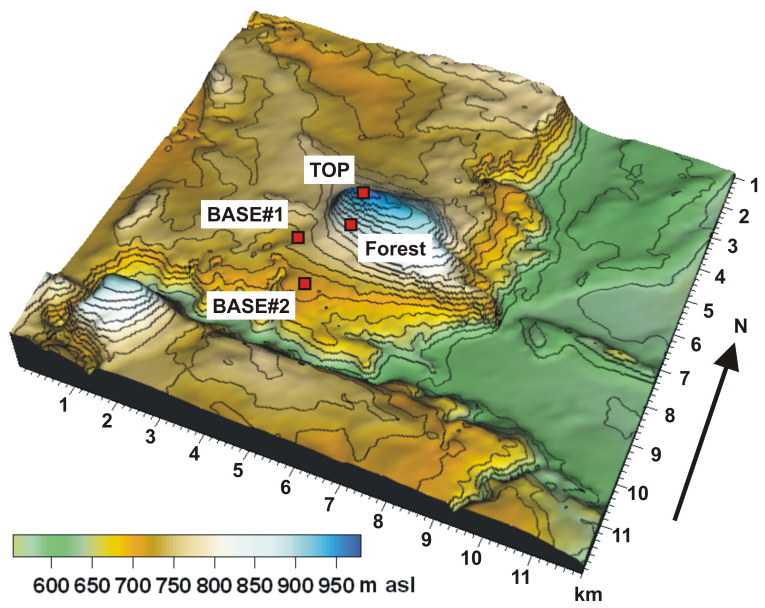


Fig. 1. Contour map of the SALSA site. Red dots indicate locations of the meteorological observatory at top of the mountain (TOP station, 998 m a.s.l.), of the Forest station (850 m a.s.l.) and of the two field stations at the foot of the mountain, stations BASE#1 (flux station, 735 m a.s.l.) and BASE#2 (sounding station, 710 m a.s.l.).

5467

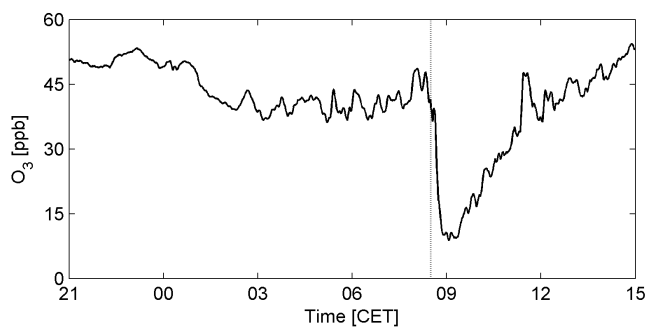


Fig. 2. Course of O₃ mixing ratio at 5 September 2005 at the TOP station. The dotted line marks the begin of the O₃ breakdown (as detected by the algorithm described in Sect. 2.5).

5468

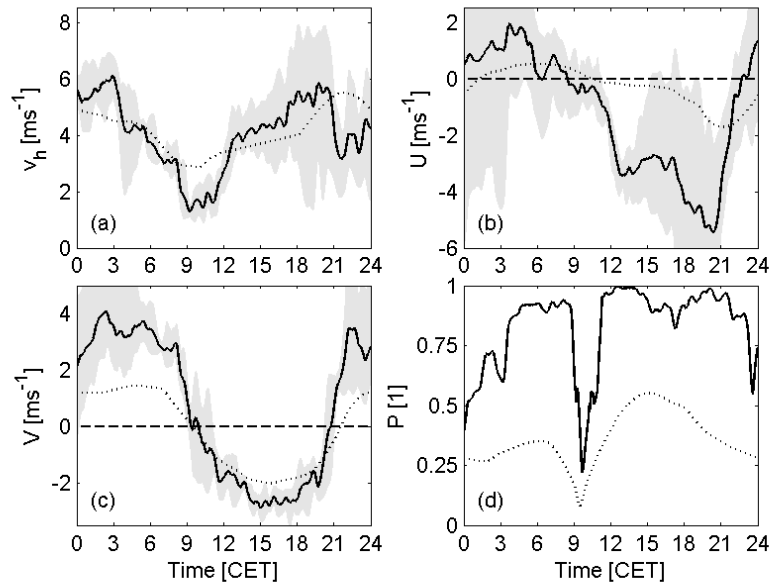


Fig. 3. Mean diurnal course of (a) scalar horizontal wind speed v_h , (b) west-east wind component U , (c) south-north wind component V and (d) persistence of wind direction P at TOP station for the last three event days (5, 7, and 8 September 2005). The grey shaded area gives the absolute range of values, the dotted line shows the corresponding result reported by Lugauer and Winkler (2005).

5469

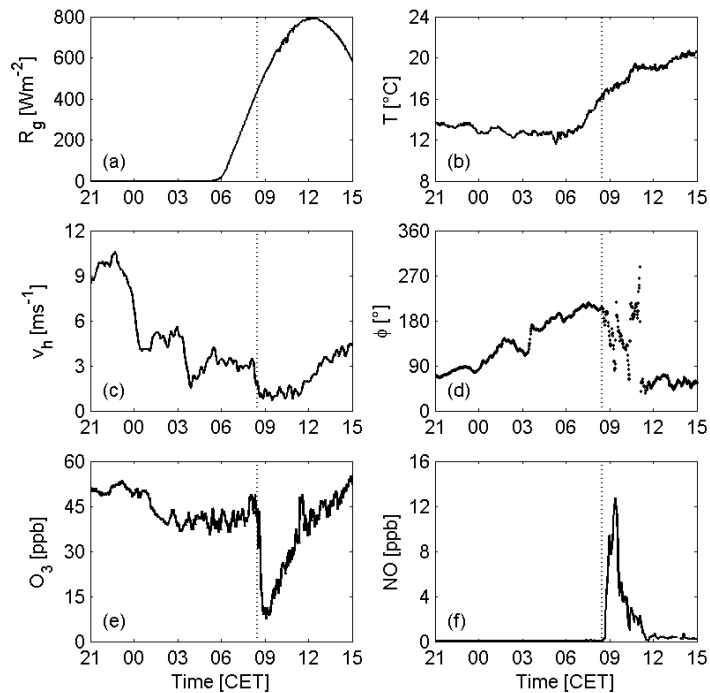


Fig. 4. Hohenpeissenberg Observatory (TOP station), 4 September 2005, 21:00 h to 5 September 2005, 15:00 h, diurnal variations of: course of (a) global radiation R_g , (b) air temperature T , (c) horizontal wind speed v_h , (d) wind direction ϕ , (e) ozone mixing ratio O_3 and (f) nitric oxide mixing ratio NO. Note the coinciding change of wind direction and the drop of O_3 mixing ratio together with the peak of NO mixing ratio. The dashed line indicates the onset of the O_3 event.

5470

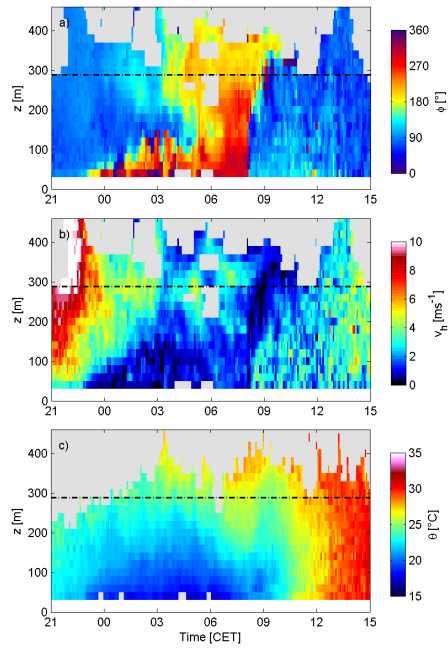


Fig. 5. Time-height cross sections of **(a)** wind direction ϕ , **(b)** horizontal wind speed v_H , and **(c)** potential air temperature θ , measured by SODAR-RASS, from 4 September 21:00 h to 5 September 15:00 h. The dash-dotted line marks the altitude of the TOP station. Note around 09:00 h the sudden change of wind direction in (a), the pronounced minimum of horizontal wind speed around the altitude of TOP in (b), and the temperature drop within the entire ABL in (c).

5471

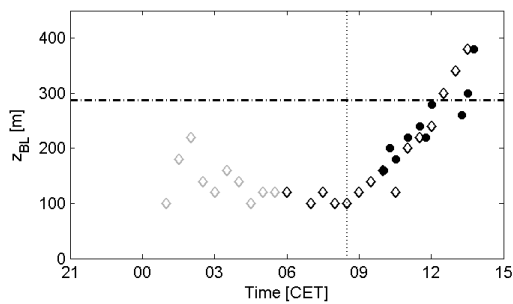


Fig. 6. Development of the BL height (z_{BL}), from 4 September 21:00 h to 5 September 15:00 h, derived from the parcel method (dots) and from secondary maximum of reflectivity (open diamonds). Grey diamonds indicate nocturnal inversion height, black diamonds indicate CBL height. The dash-dotted line marks the altitude of the TOP station, the dotted line indicates the onset of the O_3 decrease at the TOP station.

5472

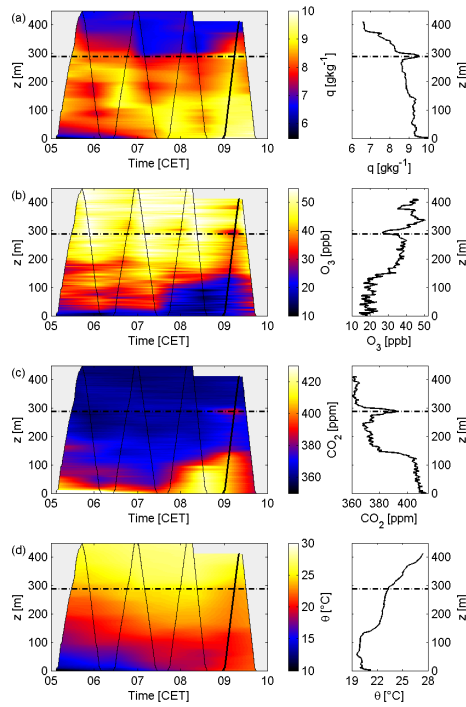


Fig. 7. Time-height cross sections and profiles of **(a)** specific humidity q , **(b)** O_3 mixing ratio, **(c)** CO_2 mixing ratio, and **(d)** potential temperature θ for the morning of 5 September 2005. The actual flight path of the tethered balloon is indicated by the thin black line. Profiles on the right side show the upward scan of the tethered balloon at the time when the O_3 drop reached the TOP station (corresponding to the actual flight path marked with a thick black line).

5473

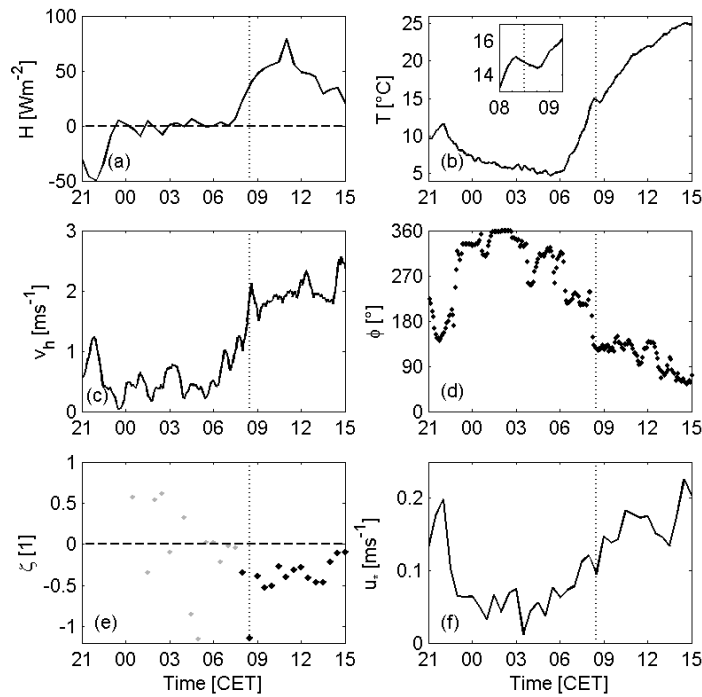


Fig. 8. Course of **(a)** sensible heat flux H , **(b)** air temperature T (exceptional drop of T enlarged), **(c)** horizontal wind speed v_h , **(d)** wind direction ϕ , **(e)** stability parameter ζ and **(f)** friction velocity u_* from 4 September 21:00 h to 5 September 15:00 h at BASE. Grey dots for ζ denote low quality of ζ due to low sensible heat flux ($-10 < H < 10$), black dots for ζ indicate high quality of derived ζ values. The dashed line indicates the onset of the O_3 event at the TOP station.

5474

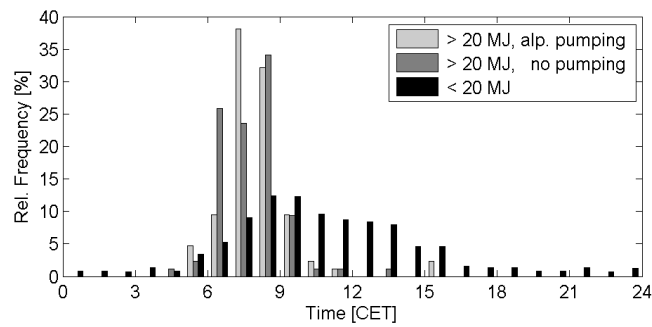


Fig. 9. Diurnal variation of relative frequency of O₃ events for days with high irradiation and Alpine Pumping (light grey, $N=84$), with high irradiation but without Alpine Pumping (dark grey, $N=85$) and for days with total irradiated energy of less than 20 MJ m⁻² (black, $N=587$).

5475

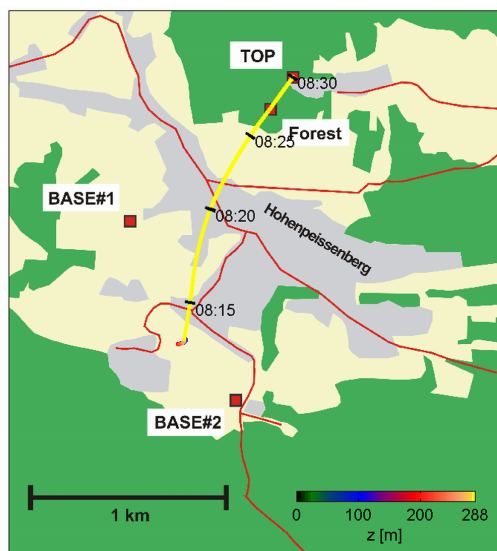


Fig. 10. Map of the village Hohenpeissenberg and the horizontal projection of a backward trajectory, computed for an impact at TOP station at 5 September 2005 08:30 h. The computed height a.g.l. of the air parcel is indicated by the colour of the trajectory. The convective ascent speed of the air mass was presumed to be in the order of 1.5 ms⁻¹ from 0 to 288 m a.g.l. (with respect to BASE#2). The wind field was based on SODAR measurements with the assumption of horizontal homogeneity. Note: the ascent needed only 3.2 min and is thus barely visible in the figure.

5476